Controlling ion kinetic energy distributions in laser produced plasma sources by means of a picosecond pulse pair

Aneta S. Stodolna, Tiago de Faria Pinto, Faisal Ali, Alex Bayerle, Dmitry Kurilovich, Jan Mathijssen, Ronnie Hoekstra, Oscar O. Versolato, Kjeld S. E. Eikema, and Stefan Witte

Citation: Journal of Applied Physics **124**, 053303 (2018); doi: 10.1063/1.5033541
View online: https://doi.org/10.1063/1.5033541
View Table of Contents: http://aip.scitation.org/toc/jap/124/5
Published by the American Institute of Physics

Controlling ion kinetic energy distributions in laser produced plasma sources by means of a picosecond pulse pair

Aneta S. Stodolna,[1,2] Tiago de Faria Pinto,[1,2] Faisal Ali,[1] Alex Bayerle,[1] Dmitry Kurilovich,[1,2] Jan Mathijssen,[1] Ronnie Hoekstra,[1,3] Oscar O. Versolato,[1] Kjeld S. E. Eikema,[1,2] and Stefan Witte[1,2,a)]

[1]*Advanced Research Center for Nanolithography (ARCNL), Science Park 110, 1098 XG Amsterdam, The Netherlands*
[2]*Department of Physics and Astronomy, Vrije Universiteit, De Boelelaan 1081, 1081 HV Amsterdam, The Netherlands*
[3]*Zernike Institute for Advanced Materials, University of Groningen, Nijenborgh 4, 9747 AG Groningen, The Netherlands*

(Received 6 April 2018; accepted 18 July 2018; published online 7 August 2018)

The effect of a pair of picosecond pulses on the ionization and deformation of a liquid tin microdroplet is studied for a range of incident pulse parameters. Faraday cups are used to measure ion kinetic energy distributions, together with high-resolution shadowgraphy to monitor target deformation and expansion. It is found that the introduction of a relatively weak first pulse results in an order-of-magnitude reduction of the number of ions with kinetic energies above 1 keV, and a strong shift of the kinetic energy distribution towards lower energies, while the expansion dynamics of the droplet can be kept similar to the single-pulse case. By controlling the relative intensity and the time delay between pairs of pulses with 52 ps duration, regimes are identified in which spherical final target shapes are combined with a reduced high-energy ion yield. The high-energy part of the observed ion distributions has been fitted with a self-similar expansion model, showing a 30-fold decrease in characteristic ion energy for pulse pairs. This combination of results is of particular importance for plasma sources of EUV radiation for nanolithography applications, in which picosecond-laser-produced target shapes can lead to significant improvements in source conversion efficiency, while a low high-energy ion yield is desirable from a source lifetime perspective.

https://doi.org/10.1063/1.5033541

I. INTRODUCTION

The next generation of lithography machines uses extreme ultraviolet (EUV) light at a wavelength of 13.5 nm. In the past two decades, a large number of theoretical and experimental studies have been conducted on possible light sources for EUV lithography,[1] including synchrotron radiation,[2,3] free-electron lasers,[4,5] plasma sources,[6–10] and high-harmonic generation.[11]

From the aforementioned solutions, a tin-based laser-produced plasma (LPP) source received the most attention due to its high conversion efficiency, robustness, and scalability,[12,13] resulting in a first commercial machine launched in 2010. In such an LPP source, a small tin droplet is ionized by an intense laser pulse to emit the requested light at 13.5 nm. Narrowband radiation around 13.5 nm comes from multiple ionic states,[14,15] Sn^{8+} to Sn^{14+}, collisionally excited by plasma electrons heated through interaction with a powerful CO_2 laser. An effective coupling between laser light and plasma occurs near the critical density, which for CO_2-laser-driven plasma is around $10^{19}\,cm^{-3}$. At the same time, the size of the EUV source cannot be too large to match the requirements for the maximum etendue.[16] The precise control of the target shape is thus crucial for the production of EUV light in an industrial setting, and numerous irradiation schemes have been explored with the aim of optimizing conversion efficiency (CE).

The expansion of the target can be achieved by deforming the tin droplet with a pre-pulse generated either by the same CO_2 laser system[17,18] or by a separate laser, typically Nd:YAG.[19–24] The latter solution reduces the amount of backscattered light and by decoupling both laser systems, it prevents instabilities and potential damage to the lasers, at the expense of added complexity in the EUV lithography machine. The interaction between a tin droplet and a nanosecond pre-pulse leads to the generation of a high-density disk target and results in a reported conversion efficiency of 4.7%.[25] Alternatively, a picosecond pre-pulse could be employed that expands the droplet to a low-density diffuse target resembling an acorn,[26,27] and is associated with higher CE up to a maximum reported value of 6%.[1]

Due to the interaction with intense laser pulses, the source emits large amounts of energetic particles. Out of this debris, the ions with kinetic energies of several keV are particularly undesirable, as they may damage the nearby multilayer mirror that collects the light emitted by the plasma, reducing its reflectivity and thus limiting its lifetime.[28] This issue is particularly relevant when using picosecond-duration

a)Email: witte@arcnl.nl

pre-pulses, which are associated with an increase in the emission of ions with multi-keV energy.[29] To mitigate the impact of ion debris, several techniques have been introduced including stopping fast ions using a buffer gas,[30,31] or to guide them away to a "dump" using a magnetic field,[32] or a combination of both.[33]

Alternatively, it may be possible to control the physical mechanism responsible for the acceleration of the produced ions to the observed high velocities. Some prior studies hint towards the feasibility of such an approach. For example, in experiments on solid tin and gadolinium targets,[34,35] the ion energy distributions were shifted significantly towards lower values. This substantial reduction of ions kinetic energy was achieved by using a pulse pair comprising a weak picosecond pulse at different wavelengths (1064 nm, 532 nm, or 355 nm) followed by a strong nanosecond pulse at 1064 nm. Recently, a similar observation has been made on droplets in a double pulse irradiation scheme comprising a 7.5 ns Nd:YAG pulse with an energy of 48 mJ followed by a 600 mJ CO_2 pulse.[36] A maximum reduction in the ion average kinetic energy by a factor of 3 was observed by delaying pulses by 164 ns.

The aforementioned experiments addressed only the influence of a plasma generated by the first pulse (pre-pulse) on the ion energy distribution originated from the second pulse (main pulse). However, in the industrially relevant case, a pre-pulse is employed to fluid-dynamically transform the droplet into an optimal target shape for high-CE LPP sources. It is an open question if multi-pulse schemes can be developed that reduce the amount of high-energy ions while still producing the optimum target shape. In this paper, we address the use of a carefully designed picosecond pulse pair as a pre-pulse to reduce the amount of fast ions and additionally to transform the droplet into the preferred acorn-shaped target.

II. EXPERIMENTAL SETUP

The experimental setup, shown schematically in Fig. 1, comprised a tin droplet generator operated at approximately 10 kHz repetition rate resulting in 30 μm diameter droplets (a detailed description of the droplet generator is given in Ref. 21). The droplets were irradiated with a picosecond pulse pair, generated by a home-built Nd:YAG laser similar to the systems presented in Refs. 37–39. It consisted of a vanadate (Nd:YVO_4) oscillator generating 1064 nm pulse trains at a 100 MHz repetition rate, with a pulse duration tunable in the range from 15 ps to 100 ps. In the experiments, the pulse duration was measured by means of autocorrelation.[40] A fiber-coupled pulse picking system comprising an acousto-optic modulator in combination with an electro-optic modulator was employed to select two pulses of the same duration at a chosen time delay $\Delta\tau$, ranging from 10 ns to 1000 ns in increments of 10 ns. This pulse-picking system also reduced the repetition rate to 10 Hz to match the data acquisition rate during the experiments. The selected pulse pair was first pre-amplified by approximately seven orders of magnitude in a bounce amplifier making use of two high-gain Nd:YVO_4 crystals, which were side-pumped with diode lasers at

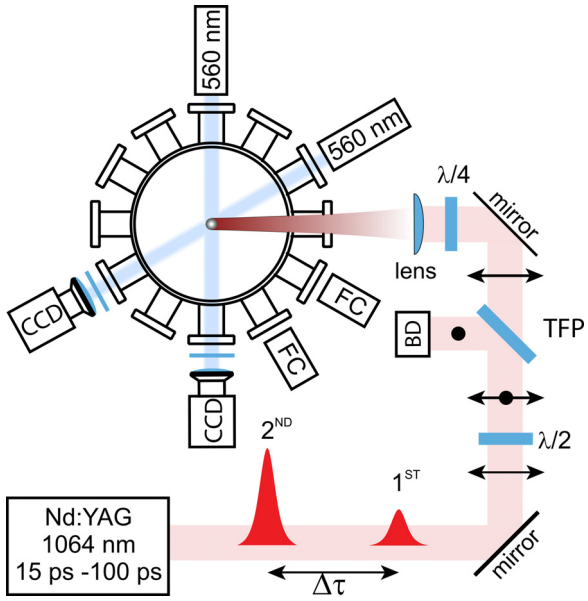

FIG. 1. A schematic representation of the experimental setup. A ps pulse pair is generated in a home-build Nd:YAG laser system with a controllable pulse duration (15 ps–100 ps) and a delay time $\Delta\tau$ between two pulses tunable from 0 to 1000 ns in increments of 10 ns. The pulse pair energy is set by means of a half-wave plate ($\lambda/2$) in combination with a thin film polarizer (TFP) and a beam dump (BD). Prior to entering the vacuum chamber, the polarization of the pulses is changed into circular with a quarter-wave plate ($\lambda/4$) and a convex lens (f = 600 mm) focuses pulses on a 30 μm tin droplet leading to the generation of plasma. The resulting ions are detected in time-of-flight measurements with Faraday cups (FC) positioned at 30° and 62° with respect to the laser plane. The time evolution of the droplet is captured on shadowgraphs obtained with two CCD cameras (at 90° and 150°) illumined by 560 nm light.

880 nm. Finally, the pulse pair was sent through a post-amplifier containing two Nd:YAG rods resulting in a maximum single pulse energy of 200 mJ. In the experiments, the energy of the pulse pair was controlled by a combination of a half-wave plate $\lambda/2$ and a thin film polarizer (TFP). The pulse energy of the second, stronger pulse was kept constant at 5 mJ whereas the energy in the first pulse was varied from 0 to 500 μJ with a Pockels cell. Prior to entering a vacuum chamber, a quarter-wave plate provided a circular polarization and a 60 cm lens focused pulses to 135 μm ($1/e^2$) at the position of the droplet. To detect the ions kinetic energy distributions, two commercial Faraday cups (FCs) (Kimball Physics, model FC-73A) were mounted at 30° and 62° with respect to the incident laser beam.[41,42] The electronic circuitry of the Faraday cups (FCs) is such that charge yields down to $10^{-4}\,\mu C\,keV^{-1}\,sr^{-1}$ can be detected for 10 keV ions. The evolution of tin droplets after the interaction with the pulse pair was recorded by means of shadowgraph images obtained from CCD cameras positioned in the horizontal plane at 90° and 150° along the laser propagation axis, allowing for a side and back view, respectively, using pulsed backlighting at 560 nm wavelength. The exposure time of the CCD cameras is set to 15 ms. By itself, this is too slow to capture the detailed target dynamics, but the actual time resolution of the shadowgraphy is determined by the backlight pulse duration of 5 ns. The camera exposure is started before the first Nd:YAG laser pulse hits the target, and the backlight laser is triggered with a controlled time

delay with respect to the Nd:YAG laser. A side effect of this imaging scheme is that the plasma glow emitted by the laser-produced plasma is also captured by the shadowgraphy camera, even though this emission occurs around $t = 0$ and fades within nanoseconds after the end of the Nd:YAG laser pulse pair.

III. RESULTS AND DISCUSSION

A series of shadowgraphs in Fig. 2 demonstrates the influence of picosecond pulses on the droplet deformation and expansion at 550 ns after the laser impact. Figure 2(a) represents a typical acorn-like shape of a droplet deformed with a single 52 ps pulse (5 mJ) which is composed of two unequal conjunct spheroids resulting from a shock wave propagation.[23,24] In brief, when an ultra-short laser pulse irradiates a tin droplet within a short amount of time (<1 ns), the light gets absorbed in a thin layer near the surface. This rapid energy deposition gives rise to a hemispherical shock wave, which focuses inside the droplet leading to cavitation and creation of the shell on the front (right) side. The second shell on the rear (left) side results from the spallation effect caused by the shock wave reflected at the back surface.

In contrast, when the same 5 mJ picosecond pulse is preceded by a weak pulse, the droplet shape changes noticeably. Remarkably, a 25 μJ pulse preceding the second pulse by 10 ns flattens the target at the front side due to plasma "push" and reduces the target expansion by 20% along the laser axis [Fig. 2(h)]. By doubling the energy in the first pulse to 50 μJ and keeping the time delay at 10 ns, more plasma is being generated, which surrounds the droplet and appears to limit its expansion at the backside as well as in the vertical direction [Fig. 2(b)]. For this compressed target, a significant reduction in spallation is observed. This may be particularly beneficial for use in LPP sources as such spalling is detrimental for machine lifetime. For longer time delays, the plasma expands and its density reduces, enabling it to again spread more in the vertical direction [Figs. 2(c) and 2(d)]. Assuming a spherical plasma expansion at constant velocity, the reduction of density for an increase in time delay from 10 ns to 50 ns is about two orders of magnitude. For time delays longer than 200 ns, the target shape reverts back to the acorn-like shape, except at the front side which stays flat as a result of a plasma generated by parasitic pulses present in the pulse train due to limited contrast of the laser setup for time delays $\Delta\tau > 100$ ns.

When the energy in the first pulse is further increased, no additional compression of the target is observed. In contrast, shadowgraphs taken for 10 ns delay show expansion in the direction of the laser light [Figs. 2(e) and 2(i)]. A possible explanation to this observation might be a shift of the position of critical density away from the droplet in the direction of the laser light with the increase in energy in the 1st pulse. Consequently, the laser light from the 2nd pulse generates plasma further away from the target permitting larger expansion of the droplet in the laser direction. A similar explanation may be used to describe the flattening of the target's front, which is visible in Figs. 2(g) and 2(j). By increasing the time delay beyond 10 ns, plasma generated by the 1st pulse has more time to fade away and the position of critical density shifts back to the vicinity of the droplet. Thus, the 2nd pulse produces plasma closer to the droplet, which experiences a stronger push at the front. The images from the back-view shadowgraphy camera oriented at 150° (data not shown) confirm that the final shapes are indeed

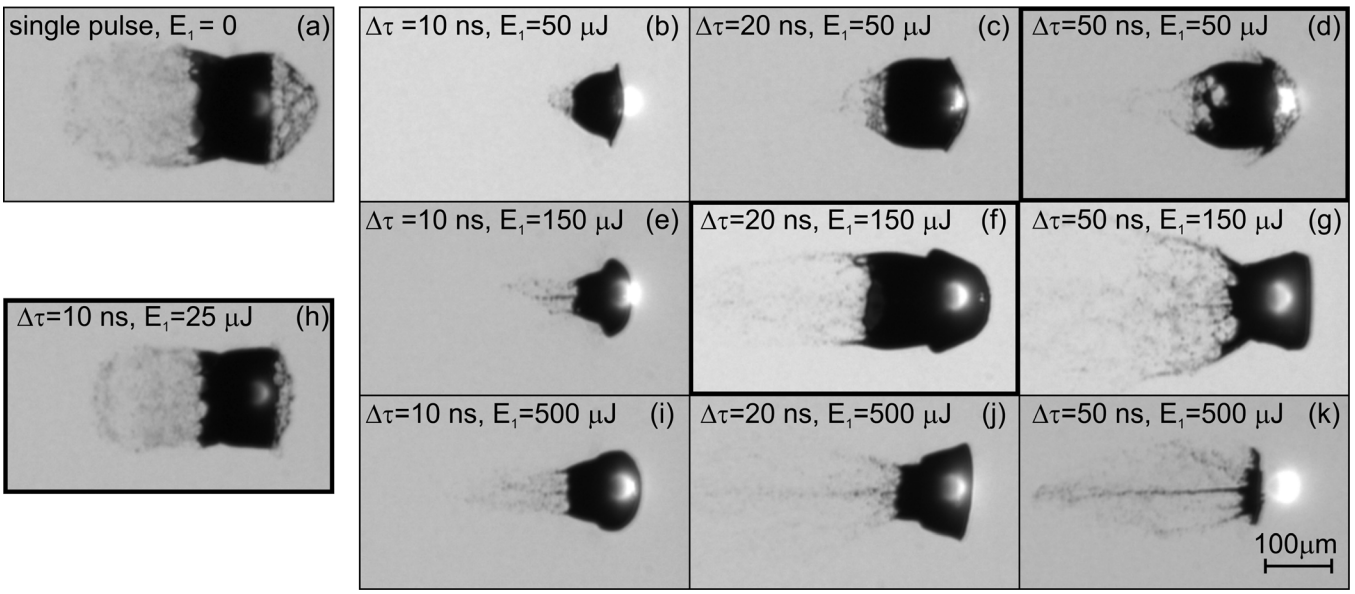

FIG. 2. Shadowgraphs showing the evolution of a 30 μm diameter tin droplet 550 ns after the interaction with a single pulse or a pulse pair for several typical parameter settings. The laser light hits the droplet from the right side and the bright spot is plasma light is captured by a camera due to the long exposure time. (a) A 52 ps single pulse with an energy of $E_2 = 5$ mJ. (b)–(d) A 52 ps pulse pair at various delay times $\Delta\tau$ with the 1st pulse energy set at $E_1 = 50$ μJ and the 2nd pulse energy fixed at $E_2 = 5$ mJ. (e)–(g) The same as (b)–(d), but with $E_1 = 150$ μJ. (h) A 52 ps pulse pair with a minimum energy in the 1st pulse of $E_1 = 25$ μJ, delayed by 10 ns with respect to the second pulse with an energy of $E_2 = 5$ mJ. (i)–(k) The same as (b)–(d), but with $E_1 = 500$ μJ. The images highlighted with a thick frame [(d), (f), and (h)] resemble a typical acorn-like shape for which the highest CE has been reported.[1] The scale bar on the bottom right holds for all panels in this figure.

similar to the single-pulse case in the transverse plane as well as along the laser propagation direction.

Different combinations of the first pulse energy (E_1) and time delay between two pulses ($\Delta\tau$) result in diverse target shapes. Nevertheless, shadowgraphs in Fig. 2 marked with a thick frame [i.e., images (d), (f), and (h)] reveal the close resemblance of some of these target shapes to the original acorn-like shape. However, as will be discussed below, the ions produced by these pulse pairs have significantly lower kinetic energies.

Figure 3(a) shows the total charge emitted in the direction of the 30° FC for different pulse pair combinations, which was calculated according to

$$\frac{dQ}{d\varepsilon} = \frac{t^3}{mL^2} \cdot \frac{I(t)}{\Omega X}, \tag{1}$$

where t is the time-of-flight, $I(t)$ is the ion current obtained by correcting the measured voltage signals for the response function of the read-out network,[41] m is the mass of tin, L is the time-of-flight distance, Ω is the solid angle, and X is the FC grid transmission. As a reference, experiments with a single pulse were performed, where the pulse energy was set to 5 mJ and the pulse duration was set to 52 ps (black symbols).

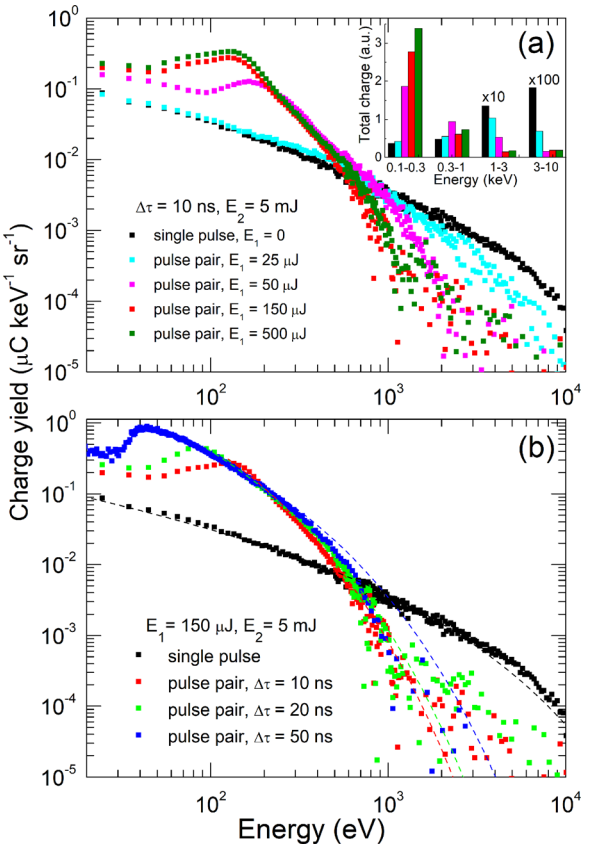

FIG. 3. (a) Charge energy distributions measured by the 30° Faraday cup resulting from the ablation of a tin droplet by a single 5 mJ, 52 ps pulse (black symbols), and by 52 ps pulse pairs delayed by 10 ns with various energies in the first pulse (E_1) and the second pulse energy set at $E_2 = 5$ mJ (colored symbols). The inset shows the total ion charge obtained by integrating the energy distributions shown in (a) in four energy ranges. (b) The effect of different time delays $\Delta\tau$ between two pulses (colored symbols) on ion energy distributions with respect to a single pulse interaction (black symbols). The dashed lines are analytical fits to the distributions according to Eq. (2).

The colored symbols correspond to measurements with pulse pairs for varying energy in the first pulse and a fixed time delay of 10 ns. The inset shows the total ion current grouped in four energy ranges. Remarkably, in the case of a pulse pair in which a first pulse with only 25 μJ energy precedes the stronger 5 mJ pulse (cyan symbols), the ion energy spectrum already shifts towards lower energies and the measured ion current in the range 3–10 keV decreases by roughly 35% compared to the single pulse case. For $E_1 = 50$ μJ (green symbols), the spectrum changes even more and the measurements demonstrate a one order of magnitude reduction in the ion current at a kinetic energy above 3 keV. However, the effect seems to saturate for energies in the 1st pulse above 150 μJ (red symbols) leading to the maximum reduction of fast ions with kinetic energies above 1 keV. In contrast, the ion current at low energies from 100 to 300 eV increases by one order of magnitude, whereas in the energy range 0.3–1 keV, this increase is only by a factor of 1.3. This growth can be explained by a geometric effect due a mismatch between the laser beam diameter (135 μm) and a tin droplet diameter (30 μm). The first pulse interacts with a droplet and generates plasma which expands well beyond 30 μm within 10 ns, resulting in a bigger target interaction area for the 2nd pulse. Our experiments on a solid tin target (manuscript in preparation), where the beam size matched the target size, show only 14% increase in the total ion current produced by a pulse pair compared to a single pulse. Therefore, by matching the beam size with the droplet, a strong reduction in the number of slow ions as well as further decrease in the number of fast ions can be expected. Furthermore, experiments on the solid target show that the absolute amount of energy in the 1st pulse determines the deceleration effect, not the percentage relation with respect to the 2nd pulse. Therefore, to induce a significant shift to the ion kinetic energy distribution, the 1st pulse needs to create a sufficiently dense plasma. Figure 3(b) shows that by keeping constant energies in both pulses, here $E_1 = 150$ μJ and $E_2 = 5$ mJ, and by delaying the pulses beyond 10 ns (colored symbols) further reduction in the ion kinetic energy is not achieved. Instead, it results in an increased current at lower kinetic energy. The signals measured with the FC oriented at 62° confirm the decrease in ion kinetic energy, albeit at a lower signal-to-noise ratio as the ion emission is strongly peaked back towards the laser.

In the single pulse case, the ion energy distribution can be explained by a self-similar model of free plasma expansion into a vacuum based on a hydrodynamic approach.[43,44] The applicability of this model for ion spectra resulting from an adiabatically expanding plasma has been recently experimentally confirmed by Bayerle *et al.*[41] The model assumes that initially a plasma occupies the half-space $x < 0$, and that the ions are cold and at rest with a step density function, whereas the electrons obey a Boltzmann distribution. Once the plasma starts to expand, the ions get accelerated in the electrostatic potential and the number of ions per unit energy and unit surface is given by[44]

$$\frac{dN}{dE} = \left(n_{i0} C_S t / \sqrt{2\varepsilon\varepsilon_0}\right) \exp\left(-\sqrt{2\varepsilon/\varepsilon_0}\right), \tag{2}$$

with n_{i0} being the initial ion density, C_S—the ion-acoustic velocity, and ε_0—the characteristic ion energy related to the electrons temperature T_e via $\varepsilon_0 = Zk_BT_e$, where Z is the ion charge number and k_B is the Boltzmann constant. As already found in previous work,[41] a fit to a self-similar expansion model that takes into account the dimensionality of the target[45] did not lead to significant improvements in the fit quality.

The dashed black line in Fig. 3(b) shows the fit of the ion kinetic energy spectrum to Eq. (2) for the single pulse case. According to the model, the plasma produced by a 52 ps single pulse at 5 mJ leads to the generation of ions with the characteristic energy of $\varepsilon_0 = 990$ (50) eV. The energy spectra recorded for pulse pairs (colored symbols) show a non-monotonic decay for the low-energy part of the spectrum with a maximum, which shifts towards lower energies when increasing the time delay between two pulses. This clearly points towards a more complex physical picture than the self-similar model provides. Nevertheless, this simplified approach can still be successfully used to describe the high-energy part of the spectrum, i.e., beyond the observed maxima. These fits, showed as colored dashed lines in Fig. 3(b), reveal that the characteristic energy is the lowest at the time delay of 10 ns (red symbols) and has a value of $\varepsilon_0 = 34.5$ (0.9) eV, which is 30 times smaller compared to the single pulse measurement. Lower values of the characteristic energy for pulse pairs hint at lower electron temperature or ion charge state Z in comparison to the single pulse case. With a single pulse, the laser light mainly interacts with the droplet, and due to its high density gets absorbed within a thin layer, leading to the generation of a hot plasma and consequently to the ejection of fast ions. For a pulse pair, the first weak pulse ablates material from a droplet, and the second pulse will therefore interact with this plasma as well as with the droplet. This second pulse may then get absorbed across a thicker layer, resulting in a colder plasma, in which the ion kinetic energies are reduced compared to the single-pulse case.

The observed changes resulting from pulse pair illumination can be considered favourable for ion mitigation by a static buffer gas, even though the present Faraday-cup-based measurements do not provide charge-state-resolved ion distributions. Buffer gas stopping of tin ions is more effective for lower charge states,[46] and any potential shift in the charge state composition for pulse pair interaction is expected to be towards such lower charge states.[47]

IV. CONCLUSIONS

The presented experimental results on laser-produced tin plasmas demonstrate that by employing a picosecond pulse pair instead of a single pulse, it is possible to greatly shift the ion kinetic energy distribution towards lower energies. Reduced kinetic energies make mitigation of the generated ions in LPPs by means of collisions with an ambient gas much more efficient.[46,48] By matching the laser beam size with the droplet size, further reduction in the number of fast ions should be achievable. Simultaneously, the recorded shadowgraphs showed that a picosecond pulse pair enables the tailoring of the target shape. Depending on the combination between the energy in the first pulse and a time delay between both pulses, it is possible to obtain shapes similar to an acorn-like target, which in the interaction with a CO_2 main pulse may lead to a higher conversion efficiency into EUV light through the opening up of a larger parameter space for optimization.

ACKNOWLEDGMENTS

This work was carried out at the Advanced Research Center for Nanolithography (ARCNL), a public-private partnership between the University of Amsterdam, the Vrije Universiteit Amsterdam, the Netherlands Organization for Scientific Research (NWO), and the semiconductor equipment manufacturer ASML.

[1]I. Fomenkov, D. Brandt, A. Ershov, A. Schafgans, Y. Tao, G. Vaschenko, S. Rokitski, M. Kats, M. Vargas, M. Purvis, R. Rafac, B. La Fontaine, S. De Dea, A. LaForge, J. Stewart, S. Chang, M. Graham, D. Riggs, T. Taylor, M. Abraham, and D. Brown, Adv. Opt. Technol. **6**, 173–186 (2017).
[2]K. Deguchi, K. Miyoshi, T. Ishii, and T. Matsuda, Jpn. J. Appl. Phys., Part 1 **31**, 2954 (1992).
[3]G. Dattoli, A. Doria, G. P. Gallerano, L. Giannessi, K. Hesch, H. O. Moser, P. L. Ottaviani, E. Pellegrin, R. Rossmanith, R. Steininger, V. Saile, and J. Wüst, Nucl. Instrum. Methods Phys. Res. Sect. A **474**, 259 (2001).
[4]Y. Socol, G. N. Kulipanov, A. N. Matveenko, O. A. Shevchenko, and N. A. Vinokurov, Phys. Rev. Spec. Top.-Accel. Beams **14**, 040702 (2011).
[5]E. R. Hosler, O. R. Wood, W. A. Barletta, P. J. S. Mangat, and M. E. Preil, *Extreme Ultraviolet EUV Lithography VI* (International Society for Optics and Photonics, 2015), p. 94220D.
[6]G. D. Kubiak, L. J. Bernardez, and K. D. Krenz, Proc. SPIE **3331**, 81 (1998).
[7]R. H. Moyer, H. Shields, A. Martos, S. W. Fornaca, R. J. S. Pierre, and M. B. Petach, *Emerging Lithographic Technologies V* (International Society for Optics and Photonics, 2001), pp. 249–255.
[8]H. Shields, S. W. Fornaca, M. B. Petach, M. Michaelian, R. D. McGregor, R. H. Moyer, and R. J. St. Pierre, Proc. SPIE **4688**, 1–8 (2002).
[9]V. Banine and R. Moors, J. Phys. Appl. Phys. **37**, 3207 (2004).
[10]M. Yoshioka, Y. Teramoto, J. Jonkers, M. C. Schürmann, R. Apetz, V. Kilian, and M. Corthout, *Extreme Ultraviolet EUV Lithography II* (International Society for Optics and Photonics, 2011), p. 79691G.
[11]E. J. Takahashi, Y. Nabekawa, and K. Midorikawa, Appl. Phys. Lett. **84**, 4 (2004).
[12]H. Mizoguchi, T. Abe, Y. Watanabe, T. Ishihara, T. Ohta, T. Hori, T. Yanagida, H. Nagano, T. Yabu, S. Nagai, G. Soumagne, A. Kurosu, K. M. Nowak, T. Suganuma, M. Moriya, K. Kakizaki, A. Sumitani, H. Kameda, H. Nakarai, and J. Fujimoto, *Extreme Ultraviolet EUV Lithography II* (International Society for Optics and Photonics, 2011), p. 796908.
[13]I. V. Fomenkov, A. I. Ershov, W. N. Partlo, D. W. Myers, D. Brown, R. L. Sandstrom, B. L. Fontaine, A. N. Bykanov, G. O. Vaschenko, O. V. Khodykin, N. R. Böwering, P. Das, V. B. Fleurov, K. Zhang, S. N. Srivastava, I. Ahmad, C. Rajyaguru, S. D. Dea, R. R. Hou, W. J. Dunstan, P. Baumgart, T. Ishihara, R. D. Simmons, R. N. Jacques, R. A. Bergstedt, and D. C. Brandt, *Extreme Ultraviolet. EUV Lithography II* (International Society for Optics and Photonics, 2011), p. 796933.
[14]G. O'Sullivan and P. K. Carroll, JOSA **71**, 227 (1981).
[15]F. Torretti, A. Windberger, A. Ryabtsev, S. Dobrodey, H. Bekker, W. Ubachs, R. Hoekstra, E. V. Kahl, J. C. Berengut, J. R. C. López-Urrutia, and O. O. Versolato, Phys. Rev. A **95**, 042503 (2017).
[16]V. Bakshi, *EUV Source for Lithography* (SPIE Press, 2006).
[17]T. Donnelly, T. Cummins, C. O. Gorman, B. Li, C. S. Harte, F. O'Reilly, E. Sokell, P. Dunne, and G. O'Sullivan, AIP Conf. Proc. **1438**, 155 (2012).
[18]K. Nishihara, A. Sunahara, A. Sasaki, M. Nunami, H. Tanuma, S. Fujioka, Y. Shimada, K. Fujima, H. Furukawa, T. Kato, F. Koike, R. More, M. Murakami, T. Nishikawa, V. Zhakhovskii, K. Gamata, A. Takata, H. Ueda, H. Nishimura, Y. Izawa, N. Miyanaga, and K. Mima, Phys. Plasmas **15**, 056708 (2008).

[19]S. Fujioka, M. Shimomura, Y. Shimada, S. Maeda, H. Sakaguchi, Y. Nakai, T. Aota, H. Nishimura, N. Ozaki, A. Sunahara, K. Nishihara, N. Miyanaga, Y. Izawa, and K. Mima, Appl. Phys. Lett. **92**, 241502 (2008).
[20]D. Hudgins, N. Gambino, B. Rollinger, and R. Abhari, J. Phys. Appl. Phys. **49**, 185205 (2016).
[21]D. Kurilovich, A. L. Klein, F. Torretti, A. Lassise, R. Hoekstra, W. Ubachs, H. Gelderblom, and O. O. Versolato, Phys. Rev. Appl. **6**, 014018 (2016).
[22]A. Y. Vinokhodov, K. N. Koshelev, V. M. Krivtsun, M. S. Krivokorytov, Y. V. Sidelnikov, V. V. Medvedev, V. O. Kompanets, A. A. Melnikov, and S. V. Chekalin, Quantum Electron. **46**, 23 (2016).
[23]M. S. Krivokorytov, A. Y. Vinokhodov, Y. V. Sidelnikov, V. M. Krivtsun, V. O. Kompanets, A. A. Lash, K. N. Koshelev, and V. V. Medvedev, Phys. Rev. E **95**, 031101 (2017).
[24]M. M. Basko, M. S. Krivokorytov, A. Yu Vinokhodov, Y. V. Sidelnikov, V. M. Krivtsun, V. V. Medvedev, D. A. Kim, V. O. Kompanets, A. A. Lash, and K. N. Koshelev, Laser Phys. Lett. **14**, 036001 (2017).
[25]J. Fujimoto, T. Hori, T. Yanagida, and H. Mizoguchi, Phys. Res. Int. **2012**, 249495 (2012).
[26]K. Tomita, Y. Sato, S. Tsukiyama, T. Eguchi, K. Uchino, K. Kouge, H. Tomuro, T. Yanagida, Y. Wada, M. Kunishima, G. Soumagne, T. Kodama, H. Mizoguchi, A. Sunahara, and K. Nishihara, Sci. Rep. **7**, 12328 (2017).
[27]Y. Kawasuji, K. M. Nowak, T. Hori, T. Okamoto, H. Tanaka, Y. Watanabe, T. Abe, T. Kodama, Y. Shiraishi, H. Nakarai, T. Yamazaki, S. Okazaki, T. Saitou, and H. Mizoguchi, Proc. SPIE **10143**, 101432G (2017).
[28]A. Takahashi, D. Nakamura, K. Tamaru, T. Akiyama, and T. Okada, Appl. Phys. B **92**, 73 (2008).
[29]B. Verhoff, S. S. Harilal, and A. Hassanein, J. Appl. Phys. **111**, 123304 (2012).
[30]D. Nakamura, K. Tamaru, Y. Hashimoto, T. Okada, H. Tanaka, and A. Takahashi, J. Appl. Phys. **102**, 123310 (2007).
[31]Y. Sun, J. Lin, X. Gao, and Z. Zhao, Sci. China Phys. Mech. Astron. **55**, 392 (2012).
[32]H. Komori, Y. Imai, G. Soumagne, T. Abe, T. Suganuma, and A. Endo, *Emerging Lithographic Technologies IX* (International Society for Optics and Photonics, 2005), pp. 859–867.
[33]S. S. Harilal, B. O'Shay, Y. Tao, and M. S. Tillack, Appl. Phys. B **86**, 547 (2007).
[34]Y. Tao, M. S. Tillack, S. S. Harilal, K. L. Sequoia, and F. Najmabadi, J. Appl. Phys. **101**, 023305 (2007).
[35]Y.-P. Dou, C.-K. Sun, C.-Z. Liu, J. Gao, Z.-Q. Hao, and J.-Q. Lin, Chin. Phys. B **23**, 075202 (2014).
[36]Z. Chen, X. Wang, D. Zuo, and J. Wang, Laser Part. Beams **34**, 552 (2016).
[37]J. Morgenweg and K. S. E. Eikema, Opt. Lett. **37**, 208 (2012).
[38]R. A. Meijer, A. S. Stodolna, K. S. E. Eikema, and S. Witte, Opt. Lett. **42**, 2758 (2017).
[39]D. W. E. Noom, S. Witte, J. Morgenweg, R. K. Altmann, and K. S. E. Eikema, Opt. Lett. **38**, 3021 (2013).
[40]B. M. van Oerle and G. J. Ernst, Appl. Opt. **35**, 5177 (1996).
[41]A. Bayerle, M. J. Deuzeman, S. van der Heijden, D. Kurilovich, T. de F. Pinto, A. Stodolna, S. Witte, K. S. E. Eikema, W. Ubachs, R. Hoekstra, and O. O. Versolato, Plasma Sources Sci. Technol. **27**, 045001 (2018).
[42]M. J. Deuzeman, A. S. Stodolna, E. E. B. Leerssen, A. Antoncecchi, N. Spook, T. Kleijntjens, J. Versluis, S. Witte, K. S. E. Eikema, W. Ubachs, R. Hoekstra, and O. O. Versolato, J. Appl. Phys. **121**, 103301 (2017).
[43]A. V. Gurevich, L. V. Pariiskaya, and L. P. Pitaevskii, JETP **22**, 449 (1966).
[44]P. Mora, Phys. Rev. Lett. **90**, 185002 (2003).
[45]M. Murakami, Y.-G. Kang, K. Nishihara, S. Fujioka, and H. Nishimura, Phys. Plasmas **12**, 062706 (2005).
[46]D. B. Abramenko, M. V. Spiridonov, P. V. Krainov, V. M. Krivtsun, D. I. Astakhov, V. V. Medvedev, M. van Kampen, D. Smeets, and K. N. Koshelev, Appl. Phys. Lett. **112**, 164102 (2018).
[47]T. Higashiguchi, M. Kaku, M. Katto, and S. Kubodera, Appl. Phys. Lett. **91**, 151503 (2007).
[48]J. F. Ziegler, J. Appl. Phys. **85**, 1249 (1999).